ACS Combinatorial Science

Research Article

pubs.acs.org/acscombsci

Combinatorial Pulsed Laser Deposition of Magnetic and Magneto-optical $Sr(Ga_xTi_yFe_{0.34-0.40})O_{3-\delta}$ Perovskite Films

Xue Yin Sun,*[,†,‡] Chen Zhang,[†,§] Nicolas M. Aimon,[†] Taichi Goto,[†] Mehmet Onbasli,[†] Dong Hun Kim,[†] Hong Kyoon Choi,[†] and C. A. Ross*[,†]

[†]Department of Materials Science and Engineering, Massachusetts Institute of Technology, Cambridge, Massachusetts 02139, United States

[‡]School of Materials Science and Engineering, Harbin Institute of Technology, Harbin 150001, People's Republic of China

[§]Singapore-MIT Alliance, National University of Singapore, 4 Engineering Drive 3, Singapore 117576

ABSTRACT: Ferromagnetic $Sr(Ga_xTi_yFe_{0.34-0.40})O_{3-\delta}$ ($0.1 \leq x, y \leq 0.5$) films with single-crystal perovskite structure were epitaxially grown on (001) $(LaAlO_3)_{0.3}(Sr_2AlTaO_6)_{0.7}$ substrates by combinatorial pulsed laser deposition (CPLD) and compared with previous results from films grown from single targets. In CPLD films the Fe was present as both Fe^{2+} and Fe^{3+}. The distribution of Sr, Ga, Ti, and O was homogeneous, but Fe-rich nanowires with diameter of 3 nm were present perpendicular to the film plane. The unit cell was tetragonally distorted with the ratio of out-of-plane to in-plane lattice parameter decreasing from 1.06 to 1.02 as the Ga content increased. The magnetic easy axis of the films changed from out-of-plane when Ti content $y > 0.3$ to isotropic as the Ga content increased, consistent with a reduction in magnetoelastic anisotropy. The Ga lowered the Faraday rotation and the magnetization but increased the optical transmittance.

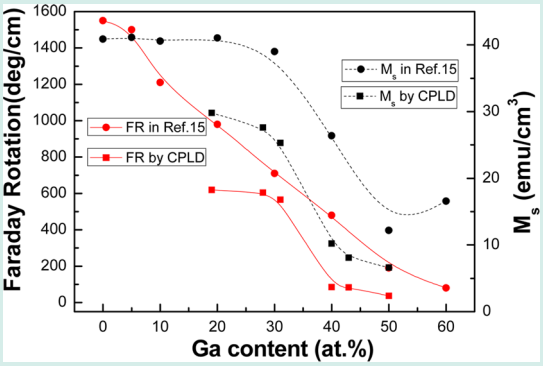

KEYWORDS: *combinatorial pulsed laser deposition, perovskite, magnetoelastic anisotropy, Faraday rotation*

INTRODUCTION

Nonreciprocal photonic devices such as optical isolators or circulators[1−3] rely on magneto-optical (MO) materials. Integrated nonreciprocal photonic devices require a MO material with not only a good figure of merit (FOM, the Faraday rotation divided by optical absorption) but the ability to be grown on a semiconductor substrate.[4,5] The most widely studied MO material in the near-IR is iron garnet,[6−11] but magnetically substituted perovskites with generic formula ABO_3 offer an alternative in which the magnetic and optical properties can be tuned by substitutions on the A and B sites.[12−17] Perovskite films can be grown epitaxially on silicon using buffer layers, and the magnetic and MO properties of several compositions have been explored, including $Sr(Ti,Fe)O_3$ (STF) and $Sr(Ti,Co)O_3$,[12−14] both of which showed room-temperature ferromagnetism, high resistivity and a significant MO effect at communications wavelengths around 1550 nm.

In our previous work, it was found that substituting Ga^{3+} on the Ti^{4+} sites of STF with 40% Fe could improve the MO performance compared to STF. Ga reduced the saturation magnetization and Faraday rotation but it also lowered the optical absorption by reducing the amount of Fe^{2+} ions present, overall enhancing the FOM at 1550 nm.[15] The ∼400 nm thick $Sr(Ga_xTi_yFe_{1-x-y})O_{3-\delta}$ (GaSTF) films were grown in vacuum by pulsed laser deposition from a single target, requiring a new target to be made for each different composition film.

Combinatorial pulsed laser deposition (CPLD) provides an efficient process to grow a set of films with a composition range under the same conditions of temperature and gas ambient.[18−21] This article describes GaSTF thin films made by CPLD including magnetic properties, cross-sectional imaging and elemental mapping of films, and compares the results with those of films made by conventional PLD from a single target. GaSTF films were made by sequentially ablating two targets: $Sr(Ga_{0.65}Fe_{0.35})O_3$ (SGF35) and $Sr(Ti_{0.60}Fe_{0.40})O_3$ (STF40). The magnetic properties of the films were measured and discussed in terms of the film composition, microstructure, and elemental distribution.

EXPERIMENTAL METHODS

$Sr(Ga_xTi_yFe_{1-x-y})O_{3-\delta}$ (GaSTF, $0.1 \leq x, y \leq 0.5$) films with single-crystal perovskite structure were grown on (001) $(LaAlO_3)_{0.3}(Sr_2AlTaO_6)_{0.7}$ (LSAT) substrates by combinatorial pulsed laser deposition from targets of $SrGa_{0.65}Fe_{0.35}O_3$ (SGF35) and $SrTi_{0.60}Fe_{0.40}O_3$ (STF40) in a Neocera PLD system. δ represents the oxygen deficiency in the films, which were grown without adding oxygen to the chamber. The substrate holder and the deposition method were the same as

Received: May 9, 2014
Revised: August 13, 2014
Published: October 8, 2014

   dx.doi.org/10.1021/co5000773 | ACS Comb. Sci. 2014, 16, 640−646

Table 1. Composition and Thickness of the Samples at Different Substrate-Holder Positions

Deposition conditions	Substrate-holder position film composition and thickness		
	1	3	5
Group 1	$Sr(Ga_{0.50}Ti_{0.10}Fe_{0.40})O_{3-\delta}$ (Ga50STF), 350 nm	$Sr(Ga_{0.40}Ti_{0.22}Fe_{0.38})O_{3-\delta}$ (Ga40STF), 340 nm	$Sr(Ga_{0.28}Ti_{0.37}Fe_{0.35})O_{3-\delta}$ (Ga28STF), 310 nm
Group 2	$Sr(Ga_{0.43}Ti_{0.18}Fe_{0.39})O_{3-\delta}$ (Ga43STF), 200 nm	$Sr(Ga_{0.31}Ti_{0.32}Fe_{0.37})O_{3-\delta}$ (Ga31STF), 240 nm	$Sr(Ga_{0.19}Ti_{0.47}Fe_{0.34})O_{3-\delta}$ (Ga19STF), 300 nm

described in ref 22. Substrates were placed on the substrate holder in three positions labeled 1, 3, and 5, such that positions 1 and 5 were 5 cm apart and 3 was at the midpoint. The area of each substrate was 5 × 5 mm^2. Both the target and the sample holder were rotated so that sample 1 was directly above the SGF35 target whereas sample 5 was above the STF40 target during deposition, ensuring that the Ga content decreased and Ti content increased from sample 1 to sample 5.

The SGF35 target was made by conventional ceramic fabrication processing from >99.9% pure $SrCO_3$, Fe_2O_3, and Ga_2O_3 powders, which were calcined at 1200 °C and finally sintered at 1250 °C in air. For the STF40 target, the mixtures of powders ($SrCO_3$, Fe_2O_3, and TiO_2) were calcined at 1250 °C for 3 h and sintered at 1400 °C for 5 h. The targets were ablated by a KrF excimer laser with wavelength of 248 nm operating at 10 Hz and a fluence of 2 J/cm^2. The substrate temperature was 630 °C, and the chamber pressure at the beginning of deposition was 3.0 × 10^{-6} Torr. The distance (D_{ST}) between substrates and the targets was 8 cm. There were two groups of samples fabricated at the same substrate temperature, D_{ST}, chamber pressure and laser parameters. Samples in group 1 were made under a deposition cycle of [STF40 100 pulses + SGF35 100 pulses] × 500, those in group 2 under [STF40 100 pulses + SGF35 50 pulses] × 500. This leads to group 1 samples being richer in Ga than group 2. The number of pulses was chosen so that less than one monolayer of perovskite was deposited from each target before moving to the other target, ensuring good mixing of cations within the film.

Phase identification and texture analysis were carried out using X-ray diffraction. Conventional $2\theta - \omega$ Bragg diffraction measurement was done on a PANalytical X'pert Pro MPD diffractometer. X-ray reciprocal space mapping (RSM) was done on a Bruker HRXRD system with Ge(022)×4 monochromator. X-ray photoelectron spectroscopy (XPS) was done on a Kratos Axis Ultraspectrometer with a monochromated Al Kα source and a hemispherical analyzer. The high resolution spectrum at the Co K-edge was measured with a pass energy of 20 eV and an energy resolution of 0.3 eV.

The cation composition of the films was measured by electron microprobe, though the oxygen deficiency δ could not be determined by this method. The thickness was measured by surface profilometry (KLA-Tencor P-16+ stylus profiler). The results are shown in Table 1, where the error in thickness and composition measurement is estimated to be less than 5%. Samples for transmission electron microscopy (TEM) observation were prepared using a focused ion beam (FEI-600), and then observed on a JEOL 2010F field emission TEM, at a 200 kV acceleration voltage. The element distribution in the sample was analyzed by STEM EDX.

Magnetic properties were characterized at room temperature by vibrating sample magnetometry (VSM) using an ADE Technologies VSM Model 1660. Faraday rotation was measured at 1550 nm wavelength on a custom apparatus at room temperature, with the field and light propagation directions perpendicular to the film. Optical transmission spectra were recorded on a Cary 500i UV−Vis−NIR Dual-Beam Spectrophotometer at 200−1700 nm wavelength.

RESULTS AND DISCUSSION

The data in Table 1 shows that the Ga content of samples decreased from sample 1 to 5, while the Ti content increased, as expected from their locations with respect to the targets during deposition. The trends in thickness across the samples indicated that the deposition rate per pulse from the SGF35 target was slightly higher than that from the STF40 target. This illustrates that to obtain a uniform film thickness across the sample series it is necessary to select conditions leading to the same thickness per cycle for each target, that is, the composition gradient and the thickness gradient are not independent.

The one-dimensional XRD scans are shown in Figure 1a−d, indicating a single-crystal perovskite structure with (001) orientation for all films and no other detectable phases present. F(00l) and S(00l) indicate diffraction peaks of the film and the substrate, respectively. The F(002) peaks were shifted to lower angle with increasing Ga content because the ionic radius of Ga^{3+} (0.62 Å) is larger than that of Ti^{4+} (0.605 Å),[23] increasing the unit cell volume with Ga content. There was no distinct splitting of the peaks indicating strain-relief, as seen in our prior work on GaSTF, but this could be due to the film thickness being below the critical thickness observed in Ref. 15. There was, however, a broadening and asymmetry of the peaks in group 1 samples which suggests an inhomogeneous strain state. The out of plane lattice parameters of the films deposited by CPLD and conventional PLD [15] are shown in Figure.1g, determined from one-dimensional XRD. The lattice parameters were calculated from the highest intensity of the peak, which in group 1 gave a lower bound to the lattice parameter due to the peak asymmetry.

Figure 1e and f shows the RSM of $Sr(Ga_{0.50}Ti_{0.10}Fe_{0.40})O_{3-\delta}$ (Ga50STF) and $Sr(Ga_{0.28}Ti_{0.37}Fe_{0.35})O_{3-\delta}$ (Ga28STF), respectively, around the asymmetric LSAT (103) peak. The lattice parameters of the substrate (LSAT) measured by RSM were 3.872 ± 0.004 Å in plane and 3.867 ± 0.004 Å out of plane, and the unit cell volume of LSAT was 57.98 ± 0.02 $Å^3$, similar to prior measurements.[15,16]

From RSM, the group 1 sample Ga28STF had a well-defined in-plane lattice parameter of a = 3.872 ± 0.004 Å, the same as that of the substrate. The out of plane lattice parameter showed a broad peak in q_z. The highest intensity corresponded to c = 4.117Å, that is, c/a = 1.063 ± 0.002 indicating considerable in-plane compressive strain, but there was also significant intensity at lower q_z corresponding to c as low as ~4.04Å. The range in diffraction angles supports the interpretation of an inhomogeneous out of plane strain in the film, as suggested by the 1D scans. The RSM and 1D XRD out-of-plane lattice parameters

dx.doi.org/10.1021/co5000773 | ACS Comb. Sci. 2014, 16, 640−646

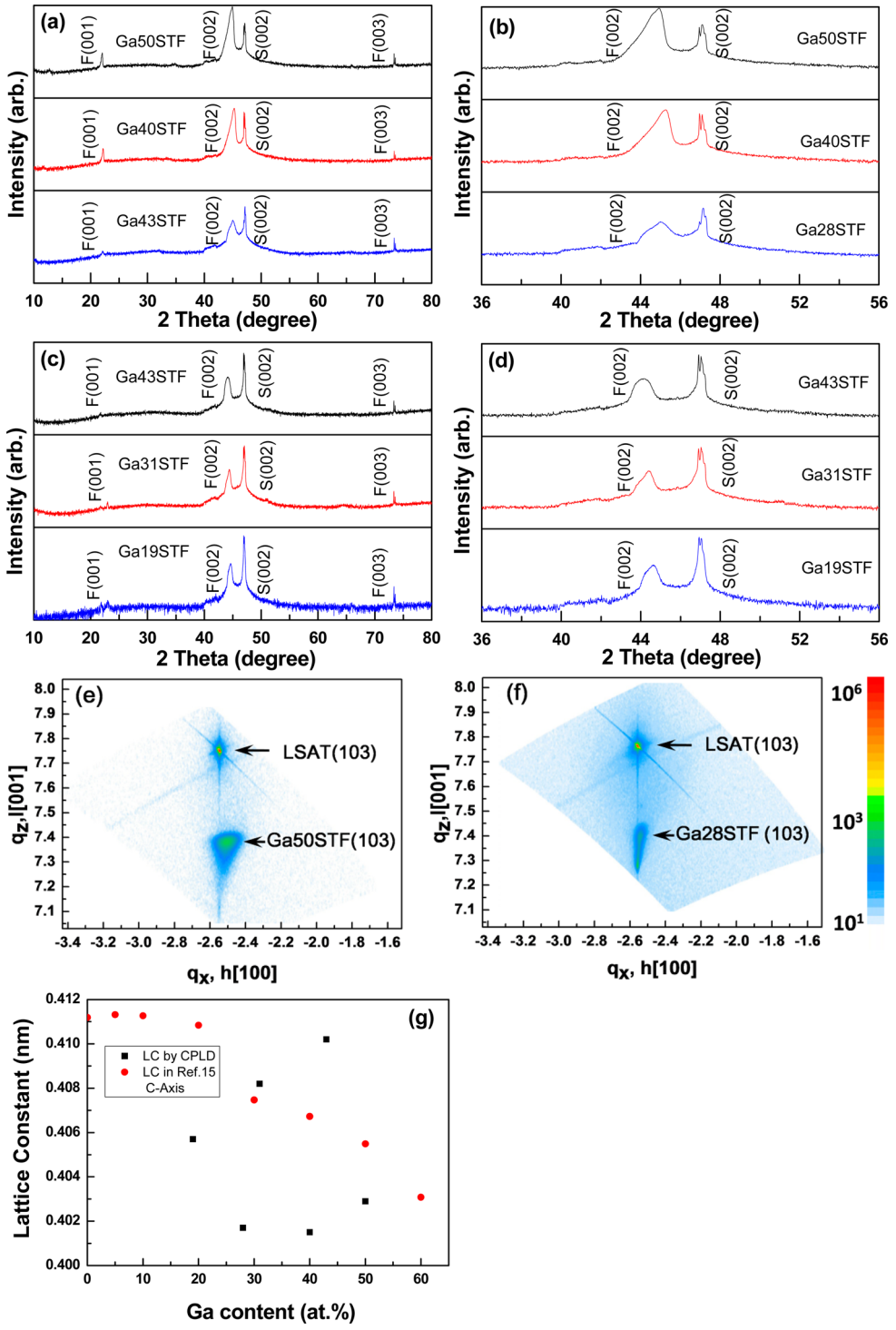

Figure 1. XRD results and X-ray reciprocal space maps of GaSTF films on LSAT. (a, b) 1DXRD $2\theta - \omega$ scans for group 1 films; (c, d) 1DXRD $2\theta - \omega$ scans for group 2 films; (e, f) X-ray reciprocal space maps of $Sr(Ga_{0.50}Ti_{0.10}Fe_{0.40})O_{3-\delta}$ (Ga50STF) and $Sr(Ga_{0.28}Ti_{0.37}Fe_{0.35})O_{3-\delta}$ (Ga28STF) respectively around the asymmetric LSAT (103) peak. The color scale indicates the peak intensity on a log scale. (g) out of plane lattice parameter of the films as function of Ga content. The three group 2 films had higher lattice parameters than the three group 1 samples.

differed, but using the peak RSM data the unit cell volume was $V = 61.724 \pm 0.02$ Å^3, i.e. the pseudocubic lattice parameter $p = V^{1/3}$ was 3.952 ± 0.004 Å.

In contrast, the Ga50STF film was partly relaxed in-plane with $a = 3.957 \pm 0.004$ Å, $c = 4.044 \pm 0.004$ Å, that is, $c/a = 1.022 \pm 0.002$, $V = 63.320 \pm 0.02$ Å^3, and $p = 3.986 \pm 0.004$ Å. The RSM peak showed less spread in q_z than that of the Ga28STF, that is, less strain inhomogeneity.

Interpolation of the 1D XRD data for the out-of-plane lattice parameter of 400 nm thick GaSTF films deposited from a single target, ref 15, yields a *c*-axis lattice parameter of 4.093 Å for Ga28STF and 4.050Å for Ga50STF. This represents a *decrease* in *c* with increasing Ga, unlike the 1D XRD data for the CPLD films. However, the unit cell volume of the films in ref 15 actually increased with Ga content because the in-plane lattice parameter *a* increased with Ga content, indicating an in-plane

dx.doi.org/10.1021/co5000773 | ACS Comb. Sci. 2014, 16, 640−646

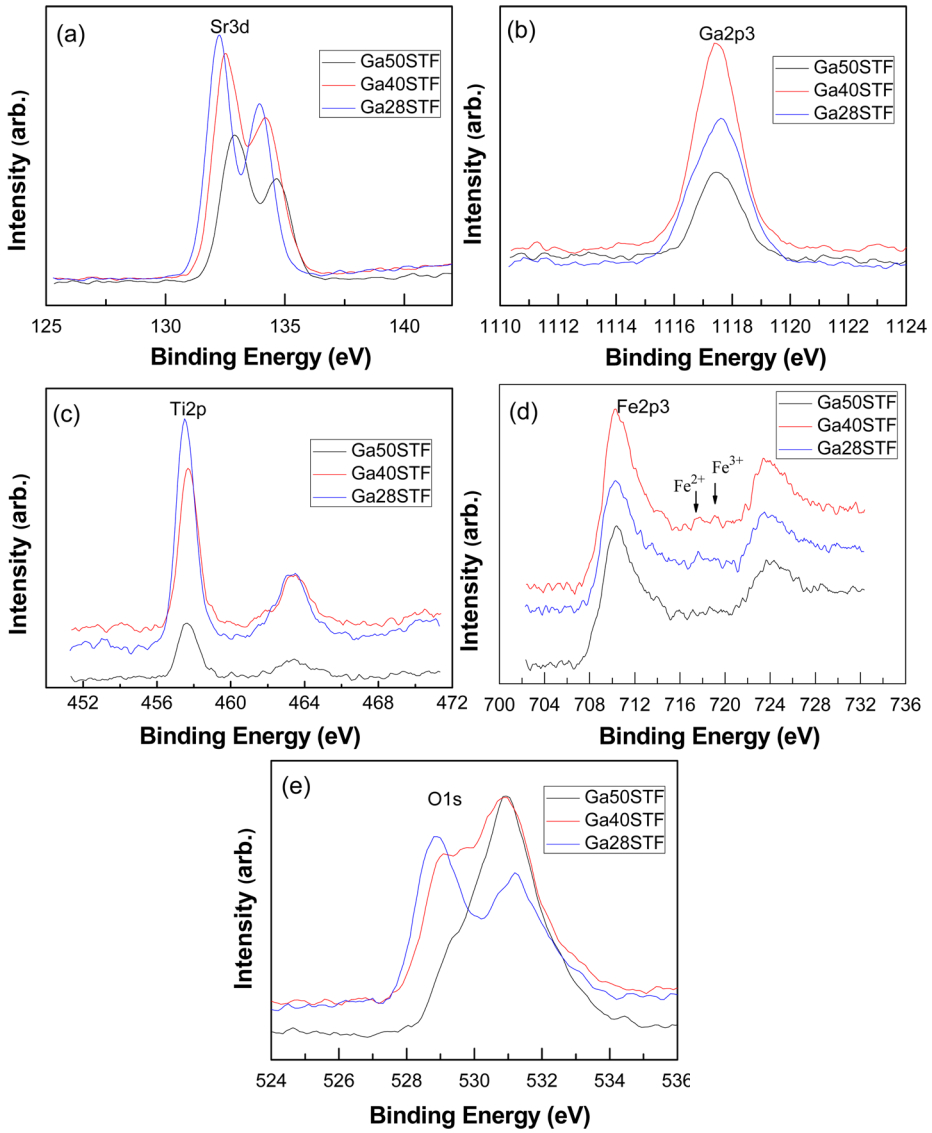

Figure 2. XPS spectra from films of $Sr(Ga_{0.50}Ti_{0.10}Fe_{0.40})O_{3-\delta}$ (Ga50STF), $Sr(Ga_{0.40}Ti_{0.22}Fe_{0.38})O_{3-\delta}$ (Ga40STF), and $Sr(Ga_{0.28}Ti_{0.37}Fe_{0.35})O_{3-\delta}$ (Ga28STF) showing the peaks of (a) Sr 3d, (b) Ga 2p, (c) Ti 2p, (d) Fe 2p, and (e) O 1s.

relaxation. Indeed, the unit cell volume increased from 59.18 Å^3 at 0% Ga to 64.62 Å^3 at 60% Ga, and the *c*/*a* ratio decreased from 1.08 at 0% Ga to 1.01 at 60% Ga in Ref. 15. The unit cell volumes from Ga28STF and Ga50STF fall between these values, even with the uncertainty in the Ga28STF *c*-parameter. The results suggest that the single-target and CPLD films had similar unit cell volumes, but there was a much greater amount of strain relaxation in the single-target films. The greater strain relaxation for the single-target films is attributed to their greater thickness than the films in the present study.

The films in group 2 showed a considerably higher out-of-plane lattice parameter than those in group 1 from 1D XRD. The peaks were more symmetrical and suggest that the films did not undergo strain relaxation, perhaps because they were thinner. If we assume the in-plane lattice parameter matched that of the substrate, the unit cell volumes (e.g., Ga19STF 60.78 Å^3, Ga43STF 61.42 Å^3) are roughly consistent with those of the group 1 samples. The data therefore show that both CPLD and single-target films have an increase in unit cell volume with Ga, but the degree of strain relaxation varies between sample sets. Whether this difference in strain relaxation is due to the lower thickness of the CPLD samples or to inherent variations between CPLD and single-target PLD is not yet known.

Figure 2 gives the XPS results of the group 1 films. Figure 2a–e shows the XPS core level spectra of Sr 3d, Ga 2p, Ti 2p, Fe 2p, and O 1s, in samples Ga50STF, $Sr(Ga_{0.40}Ti_{0.22}Fe_{0.38})O_{3-\delta}$ (Ga40STF) and Ga28STF. The binding energies (BE) were corrected by using the surface contamination C 1s peak at 285.0 eV as a reference (not shown). The C 1s peak shape and position were similar for all samples. Compared with Ga50STF, the Sr 3d peaks shifted to lower BE by 0.35 eV in Ga40STF and 0.64 eV in Ga28STF, while the BE of Ga 2p, Ti 2p did not vary. The Fe 2p results indicate that Fe was mainly present as Fe^{3+}, but there was also a Fe^{2+} peak at 717.0 eV.[24] The 719.0 eV Fe^{3+} satellite peak increased with Ga content. There was no evidence for Fe^{4+} in the GaSTF films deposited by CPLD, unlike prior work where Fe^{3+} and Fe^{4+} were found in GaSTF from a single target,[15] which might indicate a greater oxygen deficiency in the CPLD films. This would suggest that the CPLD films should have a higher unit cell volume for the same Ga content, but the uncertainties in determining unit cell volume and the other

dx.doi.org/10.1021/co5000773 | ACS Comb. Sci. 2014, 16, 640–646

differences in composition obscure any systematic observation. The main oxygen peak (O1s) was shifted toward higher BE with increasing Ga, which was attributed to an increase in oxygen vacancy concentration with Ga content.[25]

TEM images and elemental mapping of the Ga28STF film are shown in Figure 3. The film thickness was about 310 nm.

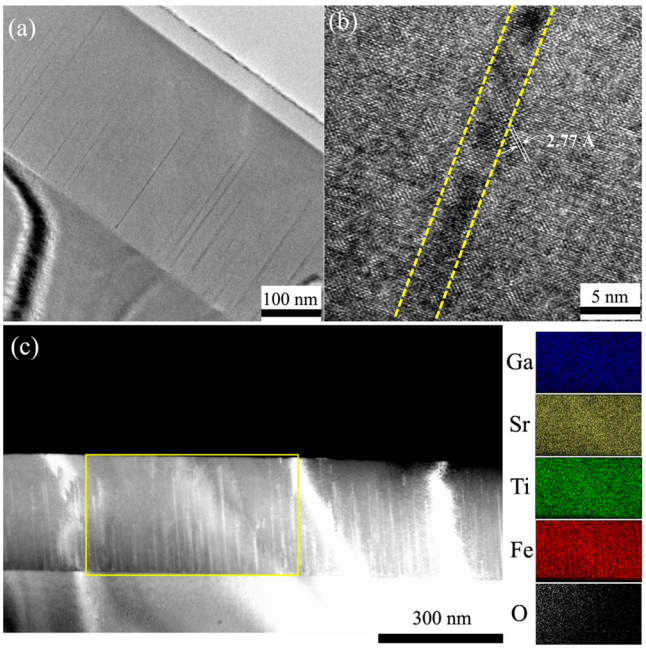

Figure 3. Transmission electron microscopy (TEM) and elemental mapping of the Ga28STF film on a (001) LSAT substrate. (a) Bright field TEM image of the film; (b) HRTEM image of a nanowire in the film (marked between the yellow lines); (c) STEM image and STEM-EDX element mapping of the film.

The film was epitaxial with narrow out-of-plane features (nanowires) of diameter ~3 nm. The spacing of the (011) planes was 2.77 Å, Figure 3a, b, consistent with the XRD lattice parameter. The elemental mapping in Figure 3c showed that the distribution of Sr, Ga, Ti, and O was homogeneous in the film but the Fe exhibited a composition modulation on the length scale of the nanowires, suggesting that the nanowires were Fe-rich. Prior work by TEM showed evidence of Fe-rich regions in single crystal $SrTi_{0.64}Fe_{0.36}O_{3-\delta}$ films,[26] but not in $Ce_{0.28}Sr_{0.72}Ti_{0.66}Fe_{0.34}O_{3-\delta}$ [16] or in $SrTi_{0.64}Fe_{0.36}O_{3-\delta}$ films with multiple crystal orientations.[26]

Magnetic hysteresis loops at room temperature are shown in Figure 4a and b. The saturation magnetization (M_s) of the films decreased from 29.8 to 6.6 emu cm^{-3} with increasing Ga. The easy axis of the films also changed, from out of plane (OP) in the lower Ga films to more isotropic for higher Ga. The hard-axis saturation field of the lower-Ga films exceeded 5−6 kOe, similar to other STF films fabricated in vacuum.[24] The decrease in net anisotropy with increasing Ga correlates with the decrease in lattice strain (c/a), which is consistent with a contribution from magnetoelastic anisotropy. Coercivity of the films was 30−70 Oe, smaller than that of films grown from a single target[15] (e.g., the coercivity of a $Sr(Ga_{0.20}Ti_{0.40}Fe_{0.40})O_{3-\delta}$ film deposited from a single target was about 100 Oe).

The Faraday rotation (FR) at 1550 nm wavelength is given in Figure 4c. The field and light propagation directions were perpendicular to the film plane. The FR loops had similar shape to the out of plane hysteresis loops in Figure 4a. The saturation FR scaled with M_s and decreased with increasing Ga. Optical transmission spectra of the films are shown in Figure 4d. The Ga enhanced the transmission of the film, similar to what was found in previous work. The saturation FR and M_s at 10 kOe of the GaSTF films as a function of Ga content is shown in Figure 4e. Both FR and M_s decreased with increasing Ga content as seen previously,[15] but the CPLD films had a lower FR and M_s than the single-target films.

Comparing the results to those of GaSTF films deposited with a single target, both methods produced single-crystal GaSTF films on LSAT. The Fe was present as mixed valence state of Fe^{2+} and Fe^{3+}, with increasing Fe^{3+} satellite peak as Ga increased. The single-target films contained Fe^{4+}, but this was not observed in the CPLD films. This presumably reflects a difference in oxygen stoichiometry, but it is not clear whether this is fundamental to the CPLD process or merely reflects variation between deposition system parameters for films grown at different times where the base pressure, plume characteristics or target condition varies. There are significant differences in the deposition process of CPLD vs single-target films, including the angle of incidence of the depositing flux, and the periodic interruptions in growth as the targets are exchanged in CPLD.

Both CPLD and single-target PLD films showed the same trend of an increase in unit cell volume and a decrease in tetragonal distortion (caused by in-plane relaxation) with increasing Ga content. The optical absorption, M_s, FR, and magnetic anisotropy all decreased with increasing Ga content. The two groups of films made with different numbers of pulses on the two targets showed significant differences in out-of-plane lattice parameter, which we attribute to a lesser amount of in-plane strain relaxation for group 2, possibly because of the lower film thickness or to process parameters, such as differences in surface mobility. The magnetic and optical properties, however, showed a monotonic change with Ga content and were insensitive to the details of the deposition sequence.

TEM revealed nanowires with diameter of 3 nm in the Ga28STF film which are believed to be Fe-rich. Metal precipitation from oxide films has been observed elsewhere, for example single-crystalline α-Fe nanowires with 30 nm diameter grew in a $LaSrFeO_4$ film deposited at 760 °C under vacuum.[27] In the GaSTF there was no clear evidence of metallic Fe from XPS, but the volume fraction of the wires may be too small to enable its detection.

CONCLUSIONS

Single-crystal GaSTF perovskite films on (001) LSAT were fabricated with a series of compositions by combinatorial pulsed laser deposition from two targets. The c/a ratio (out of plane to in-plane lattice parameter) of the GaSTF films decreased with Ga content from 1.063 in $Sr(Ga_{0.28}Ti_{0.37}Fe_{0.35})O_{3-\delta}$ to 1.022 for $Sr(Ga_{0.50}Ti_{0.10}Fe_{0.40})O_{3-\delta}$ in series 1 samples. The Fe was present as mixed valence state of Fe^{2+} and Fe^{3+}. The film with 28% Ga showed an inhomogeneous microstructure with Fe-rich nanowires of diameter of 3 nm oriented perpendicular to the film plane, although the distribution of Sr, Ga, Ti, and O were homogeneous. The higher-Ti content ($y > 0.3$) films had an out-of-plane magnetic easy axis, similar to measurements in $SrTi_{1-x}Fe_xO_{3-\delta}$, but increasing Ga content led to more isotropic behavior. The Ga enhanced the optical transmission of the film, while it lowered the saturation

dx.doi.org/10.1021/co5000773 | ACS Comb. Sci. 2014, 16, 640−646

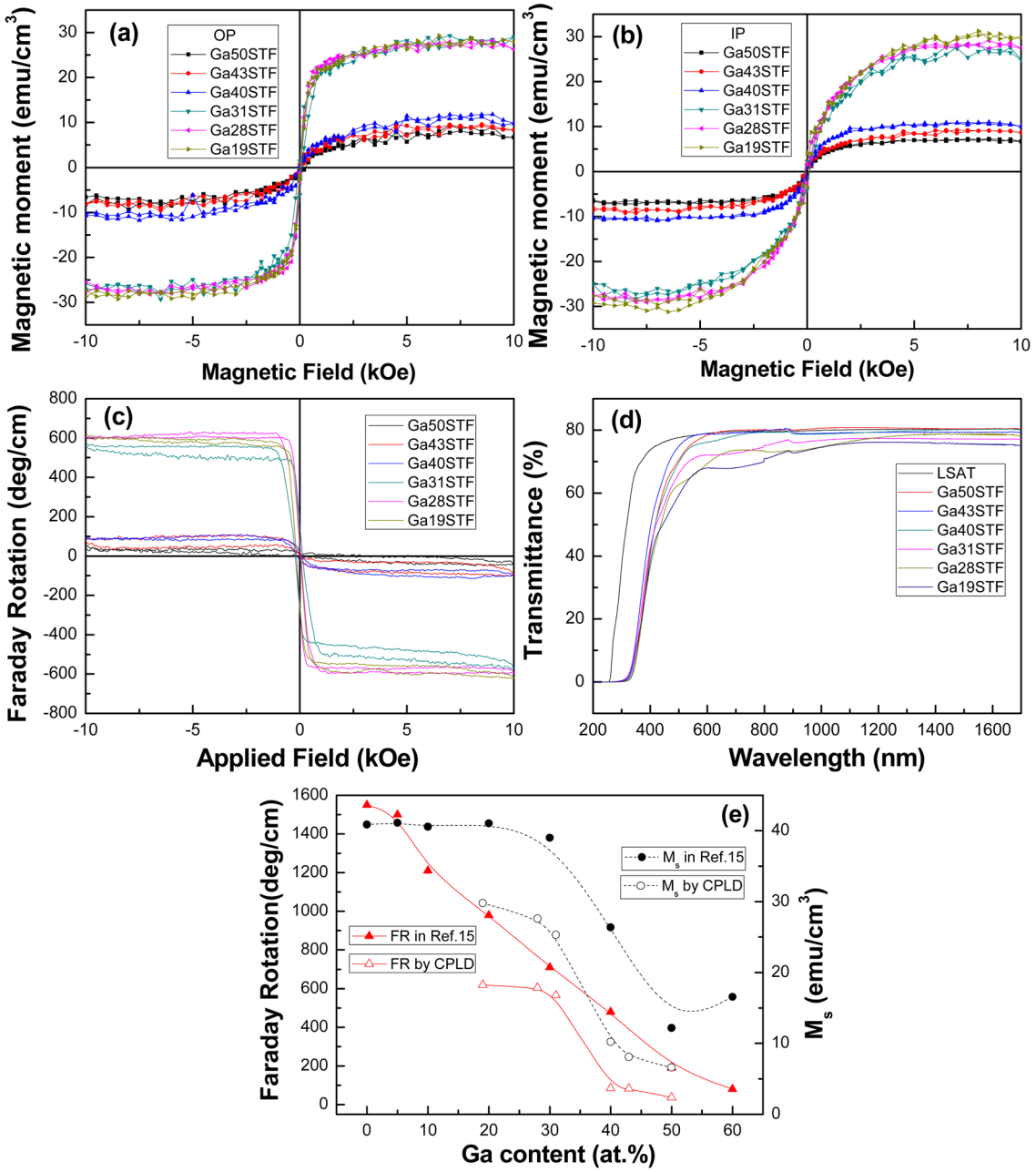

Figure 4. Properties of GaSTF films on LSAT deposited by combinatorial pulsed laser deposition at 3 μTorr and 650 °C. (a) Out-of-plane (OP) and (b) in-plane (IP) hysteresis loops of GaSTF films with different Ga content. (c) The Faraday rotation (FR) of GaSTF films measured with applied field perpendicular to the film plane at 1550 nm wavelength. (d) The optical transmission spectra of GaSTF films. (e) The saturation FR and magnetization M_s at 10 kOe as a function of Ga content.

magnetization and the Faraday Rotation. The results from combinatorial PLD show the same trends in materials properties as those from films made from a single target, despite differences in the amount of strain in the films, which supports the utility of CPLD in materials discovery.

AUTHOR INFORMATION

Corresponding Authors

*E-mail: hit2001sun@hit.edu.cn.
*E-mail: caross@mit.edu.

Notes

The authors declare no competing financial interest.

ACKNOWLEDGMENTS

This work was supported by the National Science Foundation, award DMR1104912, and FAME, a STARnet center of DARPA and MARCO. A Fellowship from the Chinese Scholarship Council (CSC) is gratefully acknowledged. This work made use of the MRSEC Shared Experimental Facilities supported by the National Science Foundation under award number DMR0819762. We thank Dr. Peng Jiang for useful discussions.

REFERENCES

(1) Bi, L.; Hu, J.; Jiang, P.; Kim, D. H.; Dionne, G. F.; Kimerling, L. C.; Ross, C. A. On-chip optical isolation in monolithically integrated non-reciprocal optical resonators. *Nat. Photonics* **2011**, *5*, 758−762.

(2) Ghosh, S.; Keyvavinia, S.; Van Roy, W.; Mizumoto, T.; Roelkens, G.; Baets, R. Ce:YIG/Silicon-on-insulator waveguide optical isolator realized by adhesive bonding. *Opt. Express* **2012**, *20*, 1839−1848.
(3) Wang, Z.; Fan, S. Optical circulators in two-dimensional magneto-optical photonic crystals. *Opt. Lett.* **2005**, *30*, 1989−1991.
(4) Yu, Z.; Fan, S. Complete optical isolation created by indirect interband photonic transitions. *Nat. Photonics* **2009**, *3*, 91−94.
(5) Zhao, W. Magneto-optic properties and sensing performance of garnet YbBi:YIG. *Sens. Actuators* **2001**, *89*, 250−254.
(6) Zhou, X.; Lin, F.; Ma, X.; Shi, W. Fabrication and magnetic properties of $Ce_1Y_2Fe_5O_{12}$ thin films on GGG and SiO_2/Si substrates. *J. Magn. Magn. Mater.* **2008**, *320*, 1817−1821.
(7) Kumar, N.; Prasad, S.; Misra, D. S.; Venkataramani, N.; Bohra, M.; Krishnan, R. The influence of substrate temperature and annealing on the properties of pulsed laser-deposited YIG films on fused quartz substrate. *J. Magn. Magn. Mater.* **2008**, *320*, 2233−2236.
(8) Goto, T.; Eto, Y.; Kobayashi, K.; Haga, Y.; Inoue, M.; Ross, C. A. Vacuum annealed cerium-substituted yttrium iron garnet films on non-garnetsubstrates for integrated optical circuits. *J. Appl. Phys.* **2013**, *113*, No. 17A939.
(9) Sung, S.; Qi, X.; Stadler, B. J. H. Integrating yttrium iron garnet onto non-garnet substrates with faster deposition rates and high reliability. *Appl. Phys. Lett.* **2005**, *87*, No. 121111.
(10) Shintaku, T.; Tate, A.; Mino, S. Ce-substituted yttrium iron garnet films prepared on $Gd_3Sc_2Ga_3O_{12}$ garnet substrates by sputter epitaxy. *Appl. Phys. Lett.* **1997**, *71*, 1640−1642.
(11) Gomi, M.; Furuyama, H.; Abe, M. Strong magneto-optical enhancement in highly Ce-substituted iron garnet films prepared by sputtering. *J. Appl. Phys.* **1991**, *70*, 7065−7067.
(12) Zhou, H. D.; Goodenough, J. B. Polaron morphologies in $SrFe_{1-x}Ti_xO_{3-\delta}$. *J. Solid. State. Chem.* **2004**, *177*, 1952−1957.
(13) Bi, L.; Kim, H.-S.; Dionne, G. F.; Ross, C. A. Structure, magnetic properties and magnetoelastic anisotropy in epitaxial $Sr(Ti_{1-x}Co_x)O_3$ films. *New. J. Phys.* **2010**, *12*, No. 043044.
(14) Kim, H.-S.; Bi, L.; Dionne, G. F.; Ross, C. A; Paik, H. J. Structure, magnetic, and optical properties, and Hall effect of Co- and Fe-doped SnO_2 films. *Phys. Rev. B.* **2008**, *77*, No. 214436.
(15) Jiang, P.; Bi, L.; Kim, D. H.; Dionne, G. F.; Ross, C. A. Enhancement of the magneto-optical performance of $SrTi_{0.6-x}Ga_xFe_{0.4}O_3$ perovskite films by Ga substitution. *Appl. Phys. Lett.* **2011**, *98*, No. 231909.
(16) Jiang, P.; Bi, L.; Sun, X. Y.; Kim, D. H.; Jiang, D.; Wu, G.; Dionne, G. F.; Ross, C. A. The effect of a-site substitution of Ce and La on the magnetic and electronic properties of $Sr(Ti_{0.6}Fe_{0.4})O_{3-\delta}$ films. *Inorg. Chem.* **2012**, *51*, 13245−13253.
(17) Kim, D. H.; Bi, L.; Jiang, P.; Dionne, G. F.; Ross, C. A. Magnetoelastic effects in $SrTi_{1-x}M_xO_3$ (M = Fe, Co, or Cr) epitaxial thin films. *Phys. Rev. B.* **2011**, *84*, No. 014416.
(18) Joshi, U. S.; Itaka, K.; Matsumoto, Y.; Koinuma, H. Combinatorial fabrication and magnetic properties of homoepitaxial Co and Li co-doped NiO thin-film nanostructures. *J. Magn. Magn. Mater.* **2009**, *321*, 3595−3599.
(19) Christen, H. M.; Silliman, S. D.; Harshavardhan, K. S. Continuous compositional-spread technique based on pulsed-laser deposition and applied to the growth of epitaxial films. *Rev. Sci. Instrum.* **2001**, *72*, 2673−2678.
(20) Yamada, Y. F.; Ohtomo, A.; Kawasaki, M. Parallel syntheses and thermoelectric properties of Ce-doped $SrTiO_3$ thin films. *Appl. Surf. Sci.* **2007**, *254*, 768−771.
(21) Venimadhav, A.; Yates, K. A.; Blamire, M. G. Scanning Raman spectroscopy for characterizing compositionally spread films. *J. Comb. Chem.* **2005**, *7*, 85−89.
(22) Aimon, N. M.; Kim, D. H.; Choi, H. K.; Ross, C. A. Deposition of epitaxial $BiFeO_3/CoFe_2O_4$ nanocomposites on (001) $SrTiO_3$ by combinatorial pulsed laser deposition. *Appl. Phys. Lett.* **2012**, *100*, No. 092901.
(23) Shannon, R. D.; Prewitt, C. T. Effective ionic radii in oxides and fluorides. *Acta Crystallogr.* **1969**, *B25*, 925−946.
(24) Kim, D. H.; Bi, L.; Aimon, N. M.; Jiang, P.; Dionne, G. F.; Ross, C. A. Combinatorial pulsed laser deposition of Fe, Cr, Mn, and Ni-substituted $SrTiO_3$ films on Si substrates. *ACS Comb. Sci.* **2012**, *14*, 179−190.
(25) Lee, Y. F.; Wu, F.; Narayan, J.; Schwartz, J. Oxygen vacancy enhanced room-temperature ferromagnetism in Sr_3SnO/c-YSZ/Si (001) heterostructures. *MRS Commun.* **2014**, *4* (1), 7−13.
(26) Kim, H. S.; Bi, L.; Kim, D. H.; Yang, D. J.; Choi, Y. J.; Jung, Woo; Lee, J. W.; Kang, J. K.; Park, Y. C.; Dionne, G. F.; Ross, C. A. Ferromagnetism in single crystal and nanocomposite $Sr(Ti,Fe)O_3$ epitaxial films. *J. Mater. Chem.* **2011**, *21*, 10364−9.
(27) Mohaddes-Ardabili, L.; Zheng, H.; Ogale, S. B.; Hannoyer, B.; Tian, W.; et al. Self-assembled single-crystal ferromagnetic iron nanowires formed by decomposition. *Nat. Mater.* **2004**, *3*, 533−538.